Microstructured superhydrorepellent surfaces: Effect of drop pressure on fakir-state stability and apparent contact angles.

L. Afferrante and G. Carbone

DIMeG Politecnico di Bari, v.le Japigia 182, 70126 Bari, Italy and

CEMeC, Politecnico di Bari, via Re David 200, 70125 Bari, Italy

Abstract

In this paper we present a generalized Cassi-Baxter equation to take into account the effect of drop pressure on the apparent contact angle θ_{app}. Also we determine the limiting pressure p_W which causes the impalement transition to the Wenzel state and the pull-off pressure p_{out} at which the drop detaches from the substrate. The calculations have been carried out for axial-symmetric pillars of three different shapes: conical, hemispherical topped and flat topped cylindrical pillars. Calculations show that, assuming the same pillar spacing, conical pillars may be more incline to undergo an impalement transition to the Wenzel state, but, on the other hand, they are characterized by a vanishing pull-off pressure which causes the drop not to adhere to the substrate and therefore to detach very easily. We infer that this property should strongly reduce the contact angle hysteresis as experimentally osberved in Ref. [21]. It is possible to combine large resistance to impalement transition (i.e. large value of p_W) and small (or even vanishing) detaching pressure p_{out} by employing cylindrical pillars with conical tips. We also show that depending on the particular pillar geometry, the effect of drop pressure on the apparent contact angle θ_{app} may be more or less significant. In particular we show that in case of conical pillars increasing the drop pressure causes a significant decrease of θ_{app} in agreement with some experimental investigations [16], whereas θ_{app} slightly increases for hemispherical or flat topped cylindrical pillars.

I. INTRODUCTION

Roughness-induced hydrophobicity is a well known effect observed in many plant leaves, e.g. Sacred Lotus leaves (*Nelumbo nucifera*) [2], and in other biological system as water striders [11] (*Gerris remigis*) or mosquito (*Culex pipiens*) eyes [12]. In all such cases the surface asperities make the liquid able to be suspended on the asperity tips, resulting in a very large contact angle (CA). The superlative water-repellency of such natural surfaces would be very appreciated in many micro- and macro- engineering applications, as liquid drops on super-hydrophobic surfaces may be very easily moved from one position to the other by simply applying an external force, resulting in the possibility to create a chemical microreactor and microfluidic microchips [13], [42]. Beside these high-tech applications, there is a strong interest of engineers in developing new commercial products as self-cleaning paints and glass windows [4], or super-hydrophobic optically transparent self-cleaning surfaces [9], [34], [35], which may be used as coatings in the automotive field, as car-windshields and biker helmets, where impacting rain drops must be easily repelled. Some studies have shown, indeed, that falling drops may fully rebound on such water-repellent surfaces with very high restitution coefficients ~ 0.9 [40]. As a consequence of the high technological and commercial impact of super-hydrophobic surfaces, in the last decade a great deal of research has been spent trying to mimic the super-hydrorepellent surfaces of living organisms. Thus, many artificial surfaces have been prepared attempting to achieve this objective. Fig. 1 shows some examples of super-hydrorepellent man-made surfaces. At a first sight, different surfaces may appear equally good candidates to mimic the super-hydrophobic properties of Natural surfaces. Indeed, being inspired by the solutions offered by Nature, several geometries have been explored, e.g. uniform arrays of flat topped cylindrical pillars [5] [Fig. 1(a)], or tapered asperities [21], [see Fig. 1(b)], or even nanotube forests with rounded tips [20] as shown in Fig. 1(c). Beside these few examples, also super-hydrophobic fractal surfaces have been produced [10]-[41], which show apparent contact angles (CAs) up to 174°. However, the different shapes of such microstructured surface, which reflect the variety of Natural solutions, should also have some practical implications which makes them not really completely equivalent. Liquid drops on super-hydrophobic microstructured surfaces may be observed mainly in two different states (although intermediate states may also exists [22], [1]) the Cassie-Baxter [7] and the Wenzel [43] states. A drop in a Cassie-Baxter state is just suspended on the asperities of the underlying surface, which therefore behaves as a fakir-carpet. The Wenzel state is, instead, characterized by complete contact between the drop and the substrate. The Wenzel state is usually unwanted as it results in a strong adherence between the drop and the substrate and in a very pronounced CA hysteresis [16], [39]. Thus, in order to prevent strong adhesion between the drop and substrate one has to design the super-hydrophobic microstructured surface in such a way to prevent the Wenzel state to be formed and make stable the fakir-droplet state. In such sense a first attempt was made in [23] where a model employing the capillary rise of a liquid in contact with a stripwise heterogeneous surface was developed to study the effect on contact angles. More recently in [3] two criteria were proposed to compare the superhydrorepellent properties of different microstuctures from a wetting point of view. However, the proposed criteria do not take into account the effect of the internal pressure of the droplet, which is strictly related to surface tension and curvature of the air-liquid spherical interface and therefore to its volume. An interesting new approach with molecular dynamics was proposed in [44], to study the behavior of liquid nanodroplets on rough surfaces. However, as shown by different authors
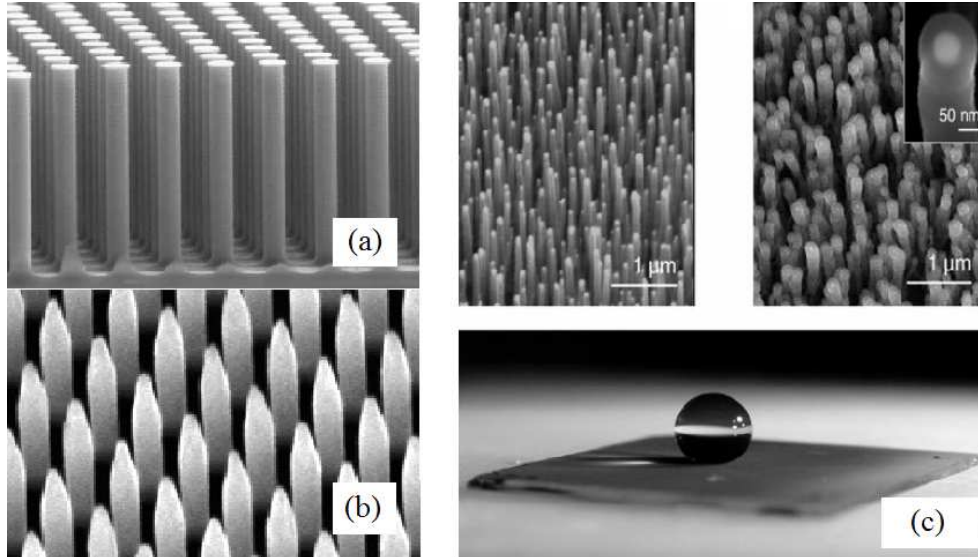
2

FIG. 1: A few examples of artifical superhydrorepellent surfaces. (a) A uniform array of very slender cylindrical pillars with a flat tip (adapted from Ref. [5]), (b) a uniform array of cylinders with tapered shaped tips (adapted form Ref. [21]), and (c) an example of superhydrorepellent carbon-nanotube forest (adapted from Ref. [20])

[16], [8], [26], [39], the drop pressure may have a critical role in determining if composite interface may be formed at the interface between the drop and the microstructured substrate. Large drop pressures may be generated during the impact of drops on the substrate, and in this case, as shown in Ref. [40], [25], [26] high impact velocities (i.e. large impact pressures) may destabilize the fakir-state, cause the transition to the Wenzel state and make the droplet not able to bounce. Fig. 2 shows indeed two water drops of the same volume on a microstructured super-hydrorepellent surface. The drop on left has been gently deposited on the substrate, thus allowing the formation of a fakir-droplet state, the drop on the right has instead undergone a transition to the Wenzel state as a consequence of an increase of the drop pressure above a critical threshold.

The transition between the composite (Cassie) and wetted (Wenzel) states has been investigated theoretically in many papers ([27], [28], [29], [30], [31], [32]), but usually the effect of the liquid drop pressure is not taken into account. Only very recently an interesting study [33] has been presented where the superhydrorepellent properties of a surface with cavities has been investigated and the effective energy of such systems has been studied by also including the influence of drop pressure. In this paper we study the system by means of an energy approach of which the most general formulation has been given by Lipowsky [17], who by means of a minimization technique proposed a generalization of the Cassie-Baxter and Wenzel laws for liquid drop sitting on chemically heterogeneous but flat substrates, where the area fraction of each phase was given a priori. Also, there are others paper treating the problem of hydraulic pressure in determining the stability of Cassie-Baxter state. [45] and [19], for example, treated this problem in the case of pillars with flat tip with sharp edges so that the fraction of the projected area that is wet is assigned a priori. In particular, [45] gave an expression of the critical hydraulic pressure for which the transition process between the Cassie-Baxter wetting mode and the Wenzel one occurs, [19] also studied the effect of the
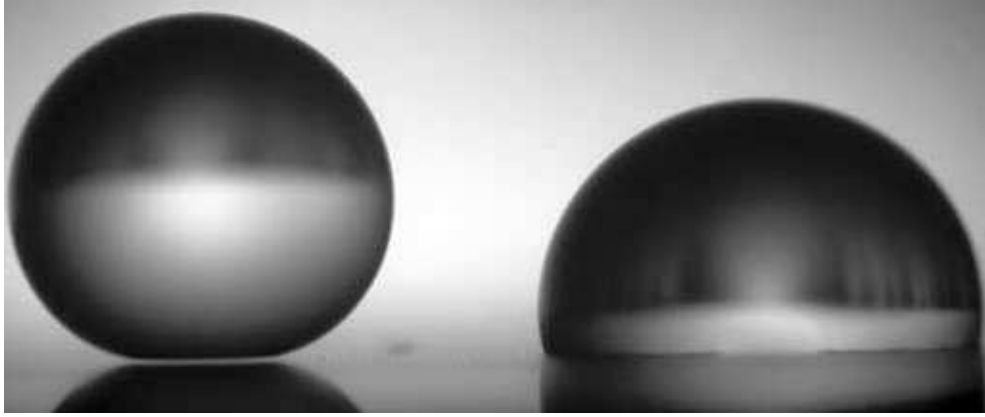
3

FIG. 2: Two millimetric water drops of the same volume on a microstructured super-hydrorepellent surface (adapted from Ref. [6]). A fakir state (i.e. Cassie-Baxter state) is obtained by gently placing the drop on the substrate (on the left). A full-contact condition (Wenzel state) is obtained by incresing the drop pressure, e.g. by let the drop impacing the surface with enough speed (on the right).

contact line length by varying the shape of the pillars while maintaining constant the area. Indeed for rounded pillars the wetted area is not fixed a priori and should be determined as a part of the problem through a minimization technique. In [18] the authors studied the case of a surface with an array of small spheres on it and determined the pressure required to force the meniscus to bend sufficiently to touch the underlying surface. However, if the pillars are sufficiently tall the transition to Wenzel state may be achieved before the meniscus touches the underlying surface because of thermodynamic instability.

In Ref. [8] it has been shown that to prevent the impalement transition it is necessary to increase the critical pressure p_W at which this transition occurs (we refer to p_W as the Wenzel pressure); high values of p_W are indeed a strict requirement in those engineering applications where rain falling drops have to be supported by the substrate. However, in many cases we also want the liquid drops be very easily detached from the substrate, i.e. the pull-off pressure p_{out} be reduced almost to zero. This property is, for example, found in many insects, that usually walk or skate on the free liquid-air surface. Such insects not only need not to sink into the water, but also need to detach easily from the liquid free and surface move and run easily on it.

In a preceding paper [8] one of the authors has analyzed the wetting/non-wetting properties of a liquid drop in contact with an extremely idealized 1D rough profile, i.e. a simple sinusoidal profile. The analysis have clarified some theoretical points (mainly from a qualitative point of view) of wetting non wetting behavior of super-hydrorepellent surfaces. Here the study is extended to 2D microstructured surfaces with periodic a distribution of axial-symmetric micropillars, which on the other hand are very commonly utilized in such applications. Some hints to design such super-hydrophobic surfaces to achieve both the aim of large p_W values and low pull-off pressures p_{out} are also provided.
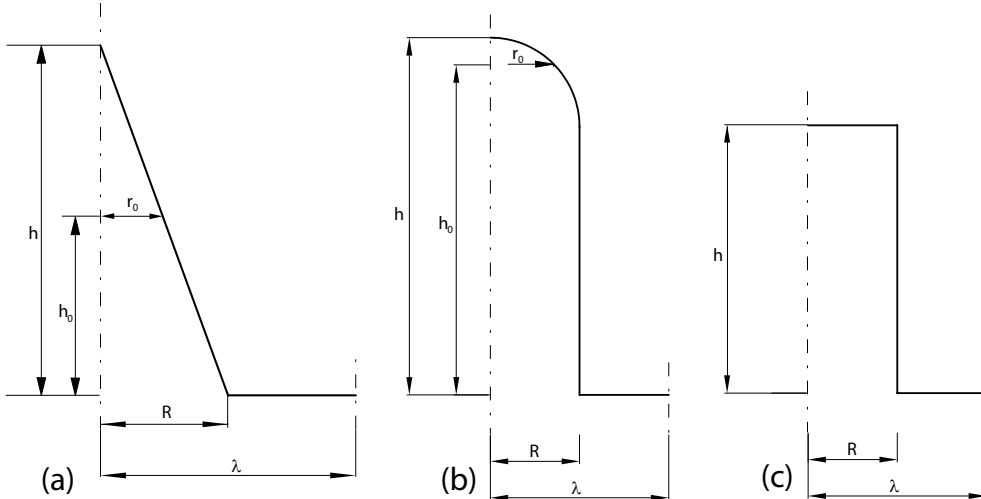
FIG. 3: Geometry of the conical (a), emispherical topped (b), and cylindrical (c), pillars.

II. FORMULATION

Let us consider a periodic distribution of chemically hydrophobic (e.g. fluorinated) pillars (thermodynamic contact angle $\theta_e > \pi/2$). We assume that the elementary cell of the periodic structure is a square, although we can deal with any type of periodic distribution of micro-pillars. We develop the analysis for three types of micro-pillars: conical pillars, hemispherical topped cylindrical pillars, and flat topped cylindrical pillars. We assume that the micropillars are stiff enough to consider negligible their deformation under the action of the drop pressure. This, indeed, is a very good approximation in many practical cases, and is always employed in theoretical investigations dealing with super-hydrorepellence. We also assume that the liquid is incompressible (i.e. we neglect the contribution of the liquid elastic energy) and the drop is very slowly evaporating (i.e. the time scale to reach the equilibrium is much shorter than the time scale of the evaporation). We observe that, being the diameter of the liquid drop in the range of millimeters, whereas the linear spacing 2λ between the pillars in the range of micro- or even nano-meters, the drop can be considered as a semi-infinite liquid space when we analyze the problem at the microscale. Thus, when we look the drop-substrate interface at very large magnifications the state of the systems is completely determined by the following state parameters: the drop-pressure p at the liquid-substrate interface, the real solid-liquid contact area, the liquid-air free surface at the interface, and the penetration Δ (see below) of the liquid drop inside the pillar forest.

Fig. 3 shows the geometry of the pillars and the parameters we use to describe the position of the triple line. The reference plane $(x, y, 0)$ is placed at the base of the pillars, and the z-coordinate is directed toward the top of the pillars. The z-coordinate of the free liquid surface will be referred to as $u(x, y)$. Because of the substrate corrugation, the liquid can either wet the whole substrate surface or be in stable or metastable partial contact with it. In case of partial contact the liquid/air interface must satisfy the Laplace formula. Assuming that the slope of the liquid-air interface is sufficiently small, which simply requires

5

that $p\lambda/\left(2\gamma_{LA}\right) \ll 1$, the Laplace formula reads

$$\nabla^2 u\left(x,y\right) = u_{xx}\left(x,y\right) + u_{yy}\left(x,y\right) = \frac{p}{\gamma_{LA}} \qquad (1)$$

where $u_{xx} = \partial^2 u/\partial x^2$, $u_{yy} = \partial^2 u/\partial y^2$ and γ_{LA} is the liquid-air surface tension. The condition $p\lambda/\left(2\gamma_{LA}\right) \ll 1$ is satisfied in most cases, e.g. in case of water $\gamma_{LA} = 72\,\mathrm{mJ/m}^2$ and assuming $\lambda \approx 1\mu\mathrm{m}$ one obtains $p < 1.4$ bar which is in most cases true. This then implies the angle which the free surface forms with the pillar, for the geometry we have investigated and $R \leq \lambda$ (where R is the radius of the pillars), need to be less than 30°.

Eq. (1), because of periodicity, can be solved over a quarter of the elementary square cell. However we need also to specify boundary conditions. A first boundary condition has to be written at the triple-line, which represents the contour delimiting the liquid-solid interface. Let us call the projection of this contour on the $\left(x,y,0\right)$ reference plane with the symbol L. We observe that, in general, the curve L (for which the mathematical expression in implicit form can be given as $f_L\left(x,y\right) = 0$) is not known *a priori* and has to be determined by requiring that the total energy of the system is stationary at equilibrium (see below). Therefore at the triple line the following equation must hold true

$$u\left(x,y\right) = h_0\left(x,y\right); \qquad \left(x,y\right) \in L \qquad (2)$$

where $L = \left\{\left(x,y\right) \in \Re^2 \mid f_L\left(x,y\right) = 0\right\}$, and $h_0\left(x,y\right)$ is the function describing the shape of the pillars. Eq. (2) simply states that the liquid-air interface and the solid-liquid interface must intersect at the triple line. Also the following Neumann boundary conditions must be satisfied to account for periodic conditions

$$u_x\left(0, y > y_0\right) = 0; \ u_x\left(\lambda, y\right) = 0$$
$$u_y\left(x > x_0, 0\right) = 0; \ u_y\left(x, \lambda\right) = 0 \qquad (3)$$

where $u_x = \partial u/\partial x$, $u_y = \partial u/\partial y$, x_0 satisfy the condition $f_L\left(x_0, 0\right) = 0$ and, similarly, y_0 satisfies the condition $f_L\left(0, y_0\right) = 0$.

Observe, that for flat topped cylindrical pillars the function $f_L\left(x,y\right)$ is known *a priori* being simply $f_L\left(x,y\right) = x^2 + y^2 - R^2$, where R is the radius of the pillar. In the other two cases $f_L\left(x,y\right)$ is not known *a priori* and must be determined as a part of the solution of the problem. Indeed, the physical problem, we are dealing with, belongs to the class of free boundary problems, and requires an additional condition to achieve the complete solution. This additional condition is simply the requirement that at equilibrium, for any given drop pressure p, the total energy of the system (in our case the Gibbs energy G) is stationary. Of course, in the general case, the Gibbs energy is a functional defined on the vector space of functions $f_L\left(x,y\right)$, and one should require that it is stationary at equilibrium to find the Euler-Lagrange equations and determine the quantity $f_L\left(x,y\right)$, making the problem belonging to the class of variational problems. Therefore, the complete solution seems to be very complicated and expensive from a numerical point of view. However we can strongly reduce the complexity of the problem if we recall that $p\lambda/\left(2\gamma_{LA}\right) \ll 1$, in such a case the slope of the free liquid-air surface is small. This implies that also the slope of the contour representing the triple line is small and we conclude that under this assumption the triple line will only negligibly deviate from a circumference in case of axial-symmetric pillars ([19] showed the variation of the angle that the free surface forms with the pillars, due to the tortuosity of the triple line, is negligible (being limited to only 3%). Thus, the unknown
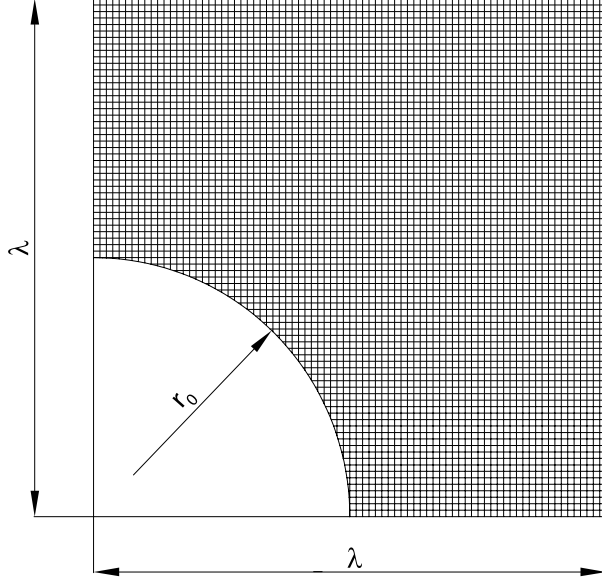
6

FIG. 4: The domain of integration of Eq. (1).

function $f_L(x,y)$ takes a much simpler form $f_L(x,y) = x^2 + y^2 - r_0^2$, where r_0 is the unknown radial position of the triple-line, and the total energy of the system simply becomes a function of the free parameter r_0. Thus, r_0 can be determined by enforcing the equilibrium condition, i.e. requiring that $\partial G / \partial r_0 = 0$. However, despite the apparent simplicity of Eq. (1), the particular shape of the domain of integration (see Fig. 4) does not make it possible to obtain a solution in closed form. We, therefore, have employed a finite difference approach to solve Eq. (1) with the mixed boundary conditions Eqs. (2) and (3).

For isothermal conditions and constant pressure the Gibbs energy is

$$G(r_0, p) = H(r_0, p) - p\lambda^2 \Delta(r_0, p) \tag{4}$$

where $\Delta(r_0, p)$ is the penetration of the rigid substrate into the semi-infinite liquid and H is the Helmholtz free energy. The penetration Δ is given by

$$\Delta(r_0, p) = h - s(r_0, p) \tag{5}$$

where s is the average profile of the liquid. Eq. (5) represents the equation of state of the system since it allows to determine one of the three quantities Δ, r_0, p once known the other two. To define the Gibbs energy we first need to express the Helmholtz free energy H which in our case is just the total surface energy of the system $H(r_0, p) = \gamma_{LS} S_{LS} + \gamma_{LA} S_{LA} + \gamma_{SA} S_{SA}$, where $\gamma_{LS} S_{LS}$, $\gamma_{LA} S_{LA}$ and $\gamma_{SA} S_{SA}$ are the surface energies at the interfaces liquid/solid, liquid/air and solid/air, respectively. Utilizing the Young's equation $\gamma_{LA} \cos\theta_e + \gamma_{LS} - \gamma_{SA} = 0$, with θ_e being the Young's CA at equilibrium, the Helmholtz free energy reads

$$H(r_0, p) = \gamma_{LA}(S_{LA} - S_{LS} \cos\theta_e) + \gamma_{SA} S_S \tag{6}$$

and the Gibbs energy becomes

$$G(r_0, p) = \gamma_{LA}(S_{LA} - S_{LS} \cos\theta_e) - p\lambda^2 \Delta + \gamma_{SA} S_S \tag{7}$$

7

In Eqs. (6) and (7) S_S represent the total surface of the substrate over the single square cell. We now require that at fixed load (i.e. at fixed drop pressure p) the Gibbs energy is stationary to enforce equilibrium conditions and close the system of equations with the following condition

$$\frac{\partial G}{\partial r_0} = 0 \qquad (8)$$

Stability or instability of equilibrium can be easily determined by looking at the sign of $\partial^2 G/\partial r_0^2$: Local stability is guaranteed when the energy has a local minimum, i.e. when $\partial^2 G/\partial r_0^2 > 0$, whereas instability is detected when $\partial^2 G/\partial r_0^2 \leq 0$.

A. The apparent contact angle

At the macroscopic scale the miscrostructure of the substrate is not observable, therefore at the macro-scale the observer will measure an apparent liquid solid surface energy $(\gamma_{LS})_{eff}$ equal to

$$(\gamma_{LS})_{eff} = H/\lambda^2 \qquad (9)$$

using Eq. (7) $(\gamma_{LS})_{eff}$ becomes

$$(\gamma_{LS})_{eff} = \frac{\gamma_{LA} \left(S_{LA} - S_{LS} \cos\theta \right)}{\lambda^2} + (\gamma_{SA})_{eff} \qquad (10)$$

where we have defined $(\gamma_{SA})_{eff} = (\gamma_{SA} S_S)/\lambda^2$ as the effective solid-air interfacial energy. At equilibrium the above definition Eq. (10) allows to write a modified Young's equation and evaluate the apparent contact angle θ_{app} as

$$\cos\theta_{app} = -\frac{(\gamma_{LS})_{eff} - (\gamma_{SA})_{eff}}{\gamma_{LA}} = -\frac{S_{LA} - S_{LS} \cos\theta}{\lambda^2} \qquad (11)$$

The above Eq. (11) represents a generalization of the Cassie-Baxter equation [7], which takes into account the influence of the interfacial drop pressure, and, of course, holds true only at equilibrium.

The above simple considerations make clear that a design criteria based on the maximization of the apparent contact angle is effective only if we include the effect of the pressure. Therefore, an optimization of the surface topography only based on the apparent contact angle evaluated by the Cassie-Baxter equation can lead to misleading conclusions.

III. EQUILIBRIUM CONDITION: A SIMPLIFIED APPROACH

The general approach considered above which leads to an optimization procedure to find Gibbs energy stationary points is very time consuming. For this reason here we present a much simpler procedure to determine the equilibrium conditions without the need of a complicated and time-consuming minimization procedure. Indeed, if we were able to enforce the equilibrium condition before solving Eq. (1), we would have the advantage of strongly reducing the complexity of the problem, since, as we are going to show, this allows to readily calculate the contact radius r_0 for any given drop pressure p and hence to 'bypass' the minimization of the Gibbs energy. This, indeed, can be done by requiring that the CA
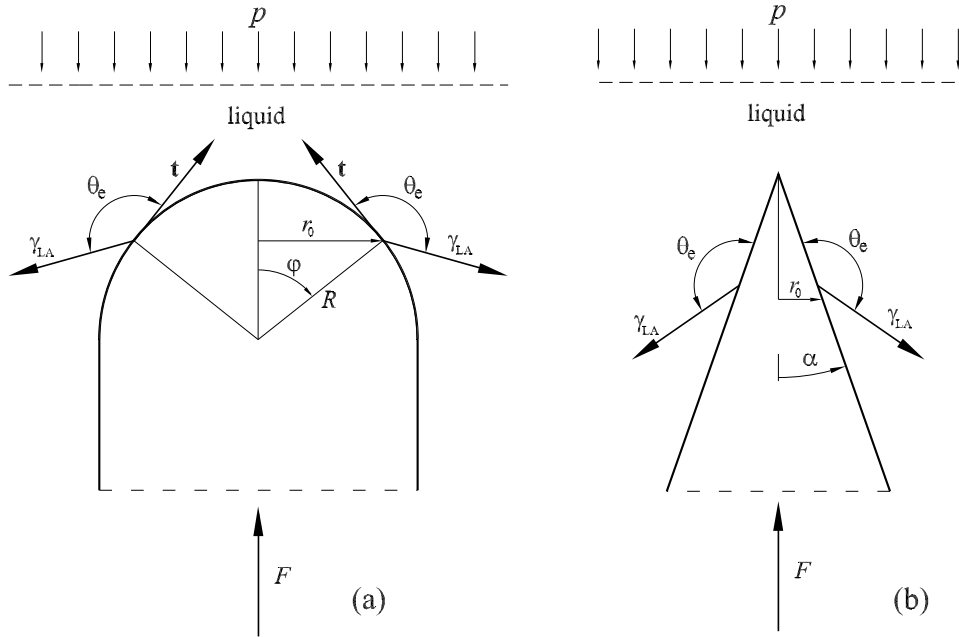
FIG. 5: The forces acting on the emispherical topped pillars, (a); and on the conical pillar, (b). Note that we have assumed that the triple line contact is circumference of radius r_0 and that the CA angle is just equal to the Young's contact angle θ_e.

at the triple line is just equal to the Young's contact angle θ_e. Therefore, as shown above, that the triple line negligibly deviates from a circumference this condition allows to calculate the real liquid-solid contact area for any given drop pressure. Of course the determination of the complete thermodynamic state of the system still requires the calculation of the free liquid-air interface $u(x, y)$ to determine the total interfacial energy and therefore the apparent contact angle θ_{eff} and penetration Δ. However, this calculation can be carried out *a posteriori* by solving Eq. (1), with the conditions (2) and (3), without handling the minimization problem of the total energy.

A.   Conical pillars

Let us observe Fig. 5 (b) where the forces acting on a conical pillar are shown to be the force F that the rigid substrate applies to the pillar, the surface tension γ_{LA} at the triple line, and the pressure p of the liquid. Thus, the equilibrium writes as

$$2\pi r_0 \gamma_{LA} \cos\left(\theta_e - \alpha\right) + F - \pi r_0^2 p = 0 \tag{12}$$

where α is the half-cone angle. Now let be A the measure of the area covered by the elementary cell (not necessarily square) of our periodic distribution of asperities, (in the case of a square cell the quantity λ is simply $\lambda = A^{1/2}/2$), and enforce the equilibrium of the whole single cell. Because of the Neumann boundary condition Eq. (3) the liquid-air surface tension at the outer boundaries of the single cell will not give any contribution to the equilibrium along the z-direction. Therefore we can write $F = pA$ and the above Eq.

(12) becomes

$$\hat{p} = -\frac{\pi \left(\hat{r}/2\right) \cos \left(\theta_e - \alpha\right)}{1 - \pi \left(\hat{r}/2\right)^2} \tag{13}$$

where $\hat{r} = r_0/\lambda$ and $\hat{p} = p\lambda/\gamma_{LA}$, being $\lambda = A^{1/2}/2$ a characteristic length. Notice when $\alpha > \theta_e - \pi/2$ the pressure becomes negative and the drop wets the substrate in a Wenzel state. Hence the angle α has to satisfy the condition $0 < \alpha < \theta_e - \pi/2$ to guarantee a positive value of the drop pressure $\hat{p} > 0$. In such case the drop pressure $\hat{p}$ continuously increases with the radius $\hat{r}$, i.e. stability of equilibrium is always guaranteed. The pull-off pressure can be easily evaluated as $\hat{p}_{out} = \hat{p}\left(\hat{r} = 0\right)$, which as shown by Eq. (13) is zero, i.e. drops on conical pillars can be very easily detached from the substrate. We observe that in all practical cases the conical tip will never present a real sharp corner. However this does not change our conclusion. The conical pillar will always guarantee a negligible pull-off pressure, as the radius of curvature of its rounded tip is always much smaller than radius of the pillar itself. Moreover, notice that since the effect of the real extension of the liquid-solid contact area on adhesion between the drop and surface is already taken into account when we calculate the contribution of the surface energy to the total energy of the system the detachment of a liquid drop from a conical pillar requires a vanishing small force even if the liquid-solid contact area can be larger than in cases of hemispherical or flat topped pillars.

B. Hemispherical topped cylindrical pillars

For hemispherical pillars (see Fig. 5 (a)), we can follow the same procedure as outlined above to write the equilibrium

$$2\pi \left(R \sin \varphi\right) \gamma_{LA} \sin \left(\theta_e + \varphi\right) + F - \pi \left(R \sin \varphi\right)^2 p = 0 \tag{14}$$

where R is the radius of the sphere and φ represents the angular coordinate of the liquid-pillar triple line [see Fig. 5(a)]. Eq. (14) can be conveniently rewritten in a dimensionless form as

$$\hat{p} = -\frac{\left(\pi/2\right) \hat{R} \sin \varphi \sin \left(\theta_e + \varphi\right)}{1 - \left(\pi/4\right) \hat{R}^2 \sin^2 \varphi} \tag{15}$$

where we have still used that $\hat{p} = p\lambda/\gamma_{LA}$ and $\hat{R} = R/\lambda$. At fixed load, stability implies $d\hat{p}/d\varphi > 0$ which is equivalent to have $\partial^2 G/\partial r_0^2 > 0$, whereas unstable equilibrium conditions are characterized by value of $d\hat{p}/d\varphi \leq 0$, i.e. $\partial^2 G/\partial r_0^2 \leq 0$. Therefore, the threshold value of pressure at which instability occurs can be determined by enforcing the condition $d\hat{p}/d\varphi = 0$, i.e.

$$-\pi \hat{R}^2 \sin \theta_e - 8 \cos \left(2\varphi\right) \sin \theta_e + \pi \hat{R}^2 \cos \left(2\varphi\right) \sin \theta_e - 8 \cos \theta_e \sin \left(2\varphi\right) = 0 \tag{16}$$

We observe that two unstable conditions can be found in general: the first one corresponds to the impalement transition to the Wenzel state and is reached when the pressure increase over a value $\hat{p}_W$ (see below), the second one is achieved when the pressure decreases below a value $\hat{p}_{out}$ which we call pull-off pressure. In particular we stress that the pull-off pressure $\hat{p}_{out}$ represents the lowest value of the pressure at which it is still possible to find a stable minimum of the total energy of the system. If the liquid pressure decreases below this threshold value the liquid drop detaches from the substrate. However the drop does not detach as a whole, but rather via the edge propagation of the triple line toward the inner
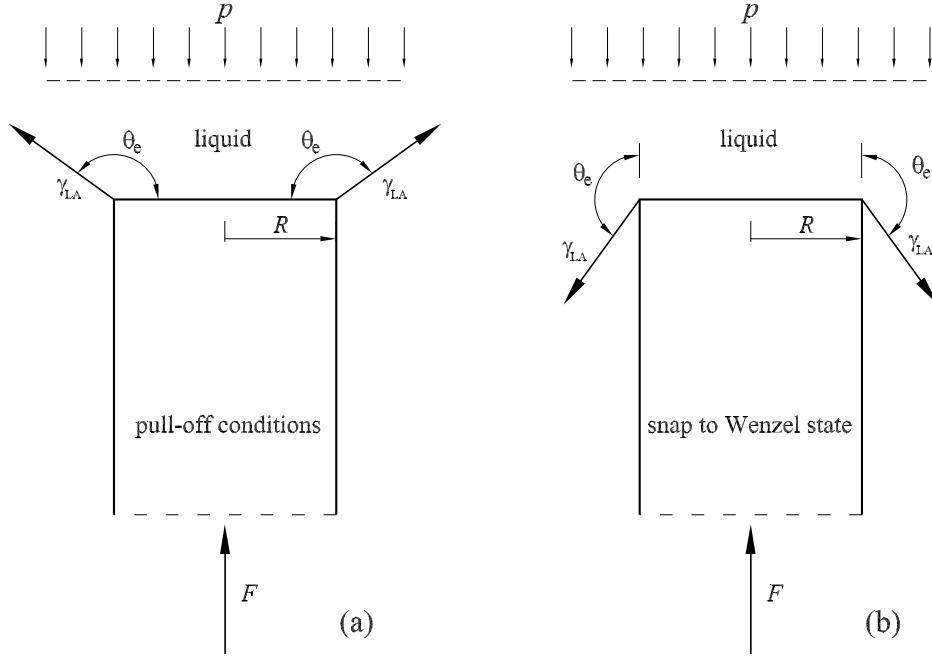
FIG. 6: The two limiting states that a liquid drop in contact with a flat-topped cylindrical pillars can assume. Limiting conditions at pull-off, (a); and limiting condition at the transition from Cassie-Baxter to Wenzel state, (b).

region of the liquid-pillar. We also observe that from a conceptual point of view, the pull-off pressure defined in the present paper is analogous to the maximum detachment force defined in Ref. [24] for capillary bridges. In fact, in our case the thermodynamic contact angle is $\theta_e > \pi/2$ and in this case the maximum detaching force for capillary bridges occurs exactly at the *transition I* point defined in Ref. [24] (see figure 5 of the cited paper). Beyond this point stable contact conditions cannot be achieved and the drop will necessarily detach from the substrate.

As in case of hemispherical topped pillars $0 < \varphi < \pi/2$, the equation $d\hat{p}/d\varphi = 0$ gives just one solution $\varphi = \varphi_{out}$, which corresponds to the pull-off condition $\hat{p}_{out} = \hat{p}(\varphi_{out})$. The impalement transition to the Wenzel state is instead obtained at $\varphi = \varphi_W = \pi/2$

$$\hat{p}_W = \hat{p}(\varphi_W) = -\cos\theta_e \frac{\pi\hat{R}/2}{1 - \pi\hat{R}^2/4} \qquad (17)$$

C. Flat topped cylindrical pillars

In case of flat topped cylindrical pillars the liquid-solid contact area on each pillar is fixed, and equal to πR^2. In such case, depending on the drop pressure values, the slope of the liquid profile at the triple line can vary between two different limiting values as clearly shown in Fig. 6. We can, therefore, easy determine the critical pressure $\hat{p}_{out}$ at pull-off [see Fig. 6(a)] as

$$\hat{p}_{out} = -\sin\theta_e \frac{\pi\hat{R}/2}{1 - \pi\hat{R}^2/4} \qquad (18)$$

11

and the critical dimensionless pressure $\hat{p}_W$ [see Fig. 6(b)] as (see also [22])

$$\hat{p}_W = -\cos\theta_e \frac{\pi\hat{R}/2}{1 - \pi\hat{R}^2/4} \tag{19}$$

which, as expected, is exactly equal to the value found for hemispherical pillars [see Eq. (17)]. It is noteworthy that, in case of flat topped cylindrical pillars, the ratio $|\hat{p}_{out}/\hat{p}_W| = \tan\theta_e$ non depending on the cylinder radius.

IV.   RESULTS

In what follows we assume that the Young's contact angle is $\theta_e = 109°$, i.e. we assume that the underlying microstructured surface is chemically hydrophobic.

A.   Conical pillars

Conical pillars have been analyzed assuming that $\hat{R} = R/\lambda = 0.5$, where R is the radius of the base circle. Fig. 7 shows the contact radius $\hat{r}$ as a function of the dimensionless drop pressure $\hat{p}$ for different values of the dimensionless pillar height $\hat{h}$. The black solid curves are obtained by Eq. (13) whereas the red-dashed ones are obtained by minimizing the total energy of the system as explained in Sec. II. Notice the very good agreement between the two approaches. Also Fig. 7 shows that $\hat{r}$ initially increase proportionally to the drop-pressure $\hat{p}$, as indeed predicted by Eq. (13), however, as the drop pressure is increased further, the contact radius also increases and the denominator in Eq. (13) may become not negligibly smaller than one. This, in turn, causes the drop pressure $\hat{p}$ to increase more than linearly with $\hat{r}$ thus explaining the deviation of curves in Fig. 7 from linearity. Since for conical pillars the partial fakir-droplet state is always stable (i.e. increasing the pressure does not force the system to undergo a spontaneous transition to the Wenzel state), a different threshold pressure $\hat{p}_L$ has to be defined. This is simply the drop pressure at which the free liquid-air interface touches for the first time the basal of the pillars. This condition, indeed, has been shown experimentally to easily trigger a sharp transition to the Wenzel state [22]. Fig. 8 shows the dimensionless limiting pressure $\hat{p}_L$ as a function of the pillar aspect ratio $\hat{h}$. Observe that increasing $\hat{h}$ also increases the limiting pressure $\hat{p}_L$, since (at fixed λ) the liquid-air interface will be farther from the bottom of the pillar. However, $\hat{p}_L$ cannot increase above the limiting asymptotic values obtained for $\hat{h} \rightarrow \infty$, i.e. $\alpha \rightarrow 0$. When this happens, the conical pillar becomes an infinitely tall cylinder of dimensionless radius $\hat{R}$ for which the Cassie-Baxter state becomes unstable when the drop-pressure reaches the values $\hat{p}_W$ given by Eq. (19) which indeed is just the asymptotic value $(\hat{p}_L)_\infty$ shown by the dashed line in Fig. 8.

Figure 9 shows the dimensionless penetration $\hat{\Delta} = \Delta/\lambda$ of the liquid drop into the pillar forest as a function of the dimensionless pressure $\hat{p}$. As expected $\hat{\Delta}$ increases as the pressure $\hat{p}$ and aspect ratio $\hat{h}$ are increased. Indeed, increasing h, at fixed R and λ, makes the cone sharper and sharper. This would in turn reduces the liquid-solid contact radius if the penetration were maintained fixed. But, since the dimensionless pressure $\hat{p}$ at equilibrium decreases if the contact radius $\hat{r}$ is reduced [see Eq. (13)], the drop actually needs to increase the penetration to increase $\hat{r}$ and, thus, sustain the applied pressure $\hat{p}$.
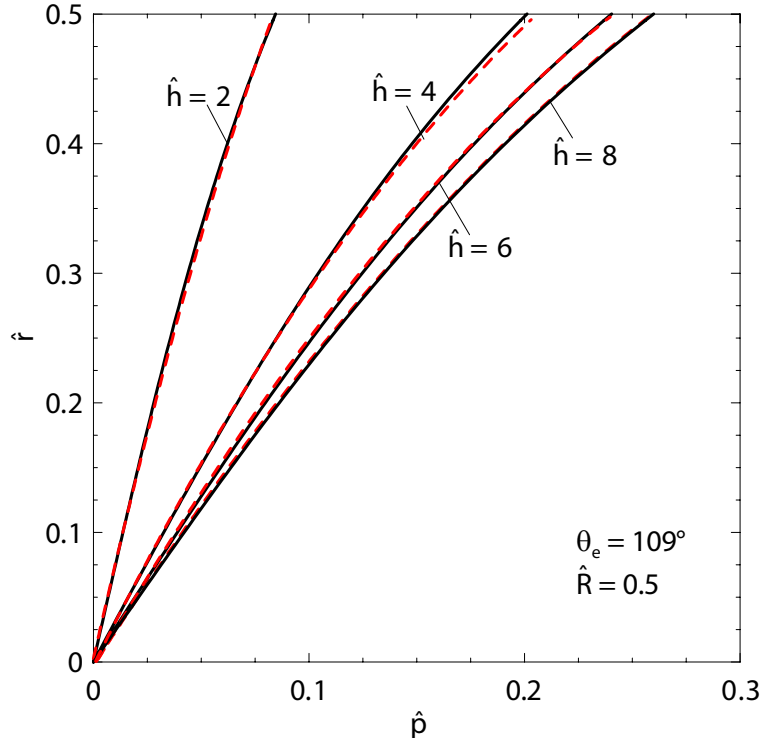
FIG. 7: The dimensionless radius of contact $\hat{r}$ as a function of the dimensionless pressure $\hat{p}$ at equilibrium, for a drop in contact with a periodic distribution of conical pillars. The red-dashed curves are results of the minimization procedure as explainen in Sec. II, black continuous lines are instead determined by the simplified approach of Sec. III. The matching between the two methodologies is excellent. Result are presented for different values of $\hat{h} = 2$, 4, 6, 8, and $\hat{R} = 0.5$, the Young's contact angle is $\theta_e = 109°$.

It is noteworthy to observe that if the dimensionless height of the conical pillar is strongly reduced, we should expect an increase, instead of a decrease, of the dimensionless penetration $\hat{\Delta}$ as a function of $\hat{h}$. Indeed, in such case the half-cone angle α would increase toward the limiting value $\theta_e - \pi/2$ at which the drop spontaneously undergoes a transition to the Wenzel state (which is obviously characterized by $\hat{\Delta} = \hat{h}$). This increase of the penetration, as a consequence of strong reduction of $\hat{h}$, is, indeed, also observed in Fig. 9 for $\hat{h} = 2$, where the corresponding $\hat{\Delta}$ values are larger than those obtained for $\hat{h} = 4$ over a large range of $\hat{p}$.

Figure 10 shows the calculated apparent contact angle θ_{app} [see Eq. (11)], as a function of the radius of the base circle $\hat{R}$ and different drop pressures $\hat{p}$. In the limit case of zero pressure $\theta_{app} = 180°$ independently of $\hat{R}$, since in this case the stable state is a perfect Cassi-Baxter state with the drop just touching the tip of the conical pillars. Increasing $\hat{p}$ the apparent contact angle decreases in qualitative agreement with some experimental observations [16]. The reason of this decrement is related to the significant increase of penetration Δ which in turn determines a strongly increase of the energy term $p\Delta$ a therefore a reduction of the apparent contact angle [see Eq. (11)]. Notice that for each given pressure $\hat{p} > 0$ a minimum value of the base radius is needed in order to stabilize the composite interface and avoid the transition to the Wenzel state. This explains why the curves at different drop pressures in
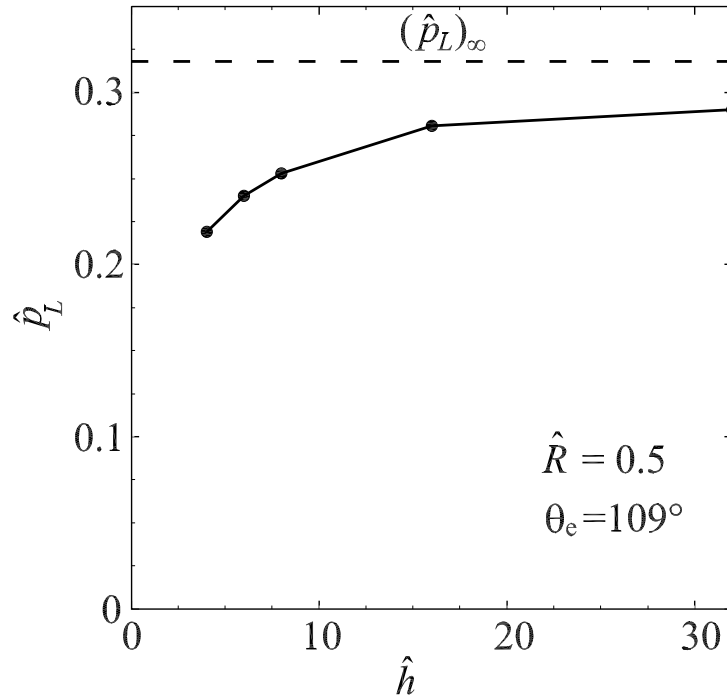
13

FIG. 8: The threshold pressure p_L as a function of the pillar aspect ratio $\hat{h}$. Results are presented for $\hat{R} = R/\lambda = 0.5$ and $\theta_e = 109°$. Observe that increasing $\hat{h}$ the limiting pressure reaches an asymptotical value $(p_L)_\infty$ which is just the values given by Eq. (17).

Fig. 10 are plotted starting from different values of the base radius $\hat{R}$.

B. Hemispherical topped pillars

To analyze the behavior of hemispherical topped pillars we use the simplified approach described in Sec. III to calculate the area of liquid-solid contact as a function of pressure, then we solve Eq. (1) to determine the shape of the free liquid-air interface and therefore the penetration of the liquid drop and the apparent contact angle. Fig. 11 shows the dimensionless liquid-pillar contact radius $\hat{r}$ at equilibrium [Fig. 11 (a)] and the dimensionless penetration $\hat{\Delta}$ [Fig. 11 (b)], as a function of the dimensionless drop pressure $\hat{p}$. Two types of lines are shown. Solid lines are stable equilibrium branches, whereas dashed lines represent unstable branches at fixed load. As expected, also in this case the contact radius and the penetration increase with the applied drop pressure, but this time the $\hat{r}$ vs. $\hat{p}$ law strongly differs from being linear. Finite negative values of $|p_{out}|$ are related to the finite size of the liquid-solid contact that still exists when the drop is about to detach from the substrate. This is often strongly unwanted since, beside the large detaching force, it usually leads also to large contact angle hysteresis [15], [38]. Also observe that for hemispherical topped cylindrical pillars impalement transition occurs spontaneously when the drop pressure reaches the limiting value p_W (at which the penetration $\hat{\Delta}$ jumps to $\hat{h}$), in contrast with what we have found for the conical pillars. Therefore, for hemispherical pillars the height should be chosen by taking care that at $p = p_W$ the free liquid-air interface does not touch the bottom
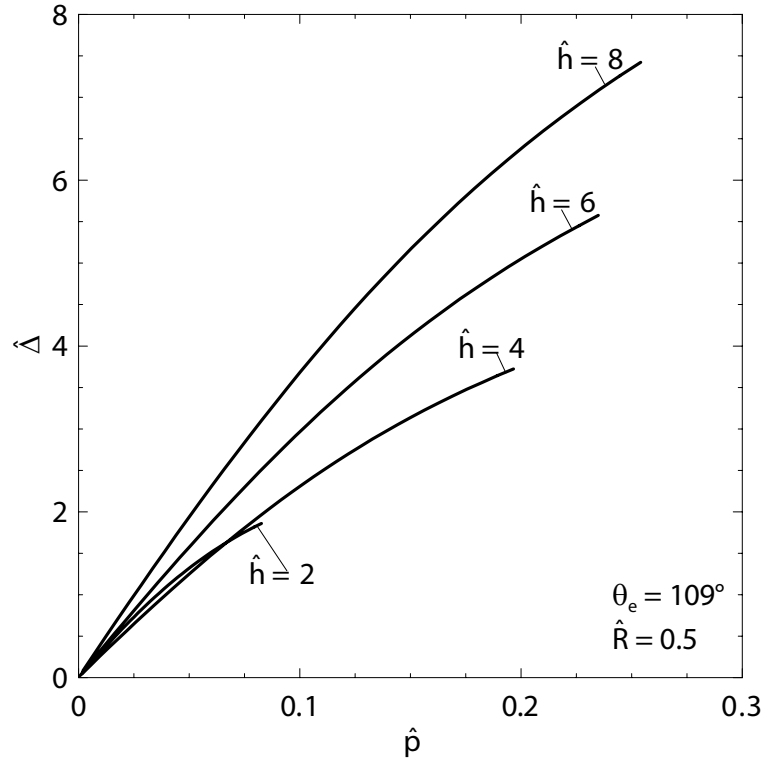
14

FIG. 9: The dimensionless drop penetration $\hat{\Delta}$, as a function of the drop pressure $\hat{p}$. Results are presented for $\hat{R} = 0.5$ and $\theta_e = 109°$, and for different values of the conical pillars aspect ratio $\hat{h}$ = 2, 4, 6, 8.
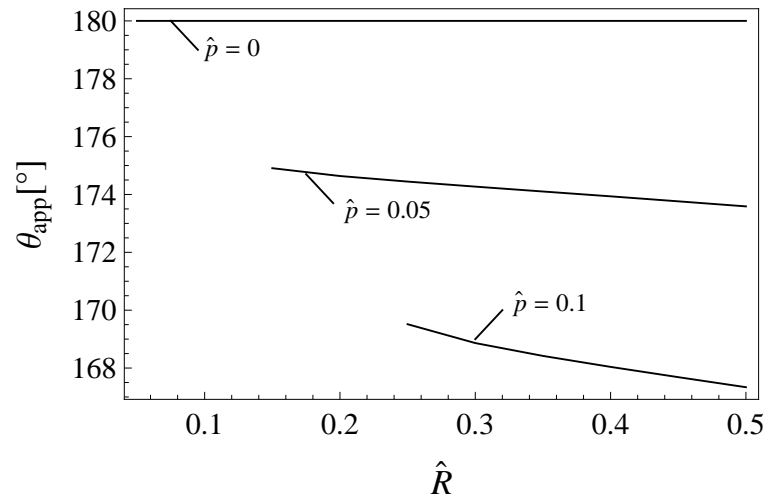

FIG. 10: The apparent contact angle θ_{app} as a function of the base radius $\hat{R}$ for conical pillars. Results are shown for different drop pressures $\hat{p}$. The aspect ratio of conical pillars is $\hat{h} = 8$.
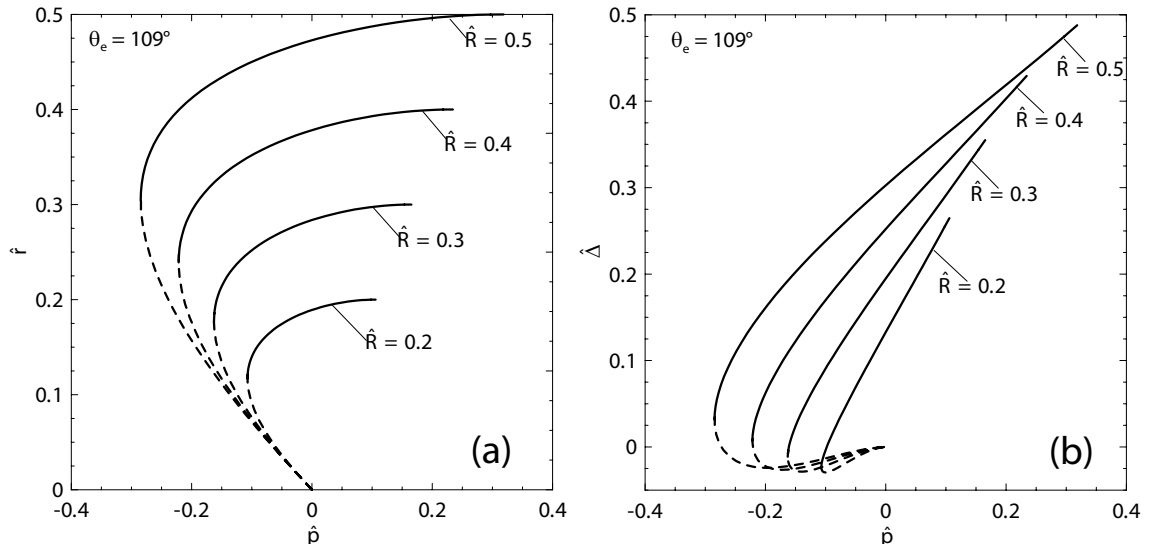
FIG. 11: The dimensionless radius $\hat{r}$ at equilibrium, (a); and the dimensionless penetration $\hat{\Delta}$ at equilibrium, (b); as a function of the dimensionless drop pressure $\hat{p}$ for hemispherical pillars. Full lines are stable branches, wherease dashed lines are unstable branches at fixed load (at fixed penetration the stability extends till to the point where $\hat{\Delta}$ has a minimum). Results are presented for different values of the dimensionless sphere radius $\hat{R} = 0.2, 0.3, 0.4, 0.5$ and for $\theta_e = 109°$. Each curve ends at a certain value of $\hat{p} = \hat{p}_W$, which only depends on the pillar radius and contact angle θ_e. When this value of drop pressure is reached the penetration sharply jumps to the unit value, i.e. the drop ungergoes a sharp transition to the Wenzel state.

of the pillars forest.

In case of hemispherical topped pillars, Fig. 12 shows that the apparent contact angle slightly increases with pressure $\hat{p}$ because in this case the liquid/air surface term $\gamma_{LA}S_{LA}$ increases more than the other two energy terms $p\lambda^2\Delta$ and $\gamma_{LS}S_{LS}$. Fig. 12 also shows the original Cassie-Baxter solution which corresponds to $\hat{p} = 0$.

C. Flat topped cylindrical pillars

In this case, for any value of the drop-pressure between the two limits p_{out} given by Eq. (18) and p_W given by Eq. (19), the contact liquid-pillar area will be always equal to πR^2 with R the radius of the cylinder. This makes the problem (1) (2) and (3) linear, and, in turn, leads to a direct proportionality between the drop pressure p and the penetration Δ, as indeed confirmed experimentally in Ref. [22]. Notice that, since $|p_{out}/p_W| = |\tan\theta_e|$ and θ_e is usually not larger than 120°, the pull-off pressure is always larger than p_W. Therefore we expect that, although a forest of flat topped cylinders can stabilize the Cassi-Baxter state, a drop suspended on such a microstructured surface is relatively difficult to detach from it and should suffer of strong contact angle hysteresis.

Fig. (13) shows the variation of the apparent contact angle θ_{app} as a function of the cylinder radius $\hat{R}$ for different drop pressures. Similarly to the case of hemispherical pillars the apparent contact angle grows with the pressure, although in this case this increment is
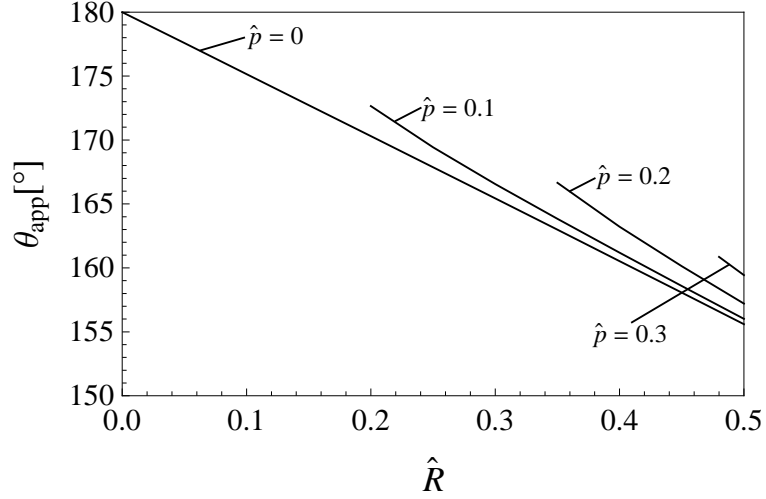
16

FIG. 12: The apparent contact angle θ_{app} as a function of the radius $\hat{R}$ for hemispherical topped pillars. Results are shown for different dimensionless drop pressure $\hat{p}$.
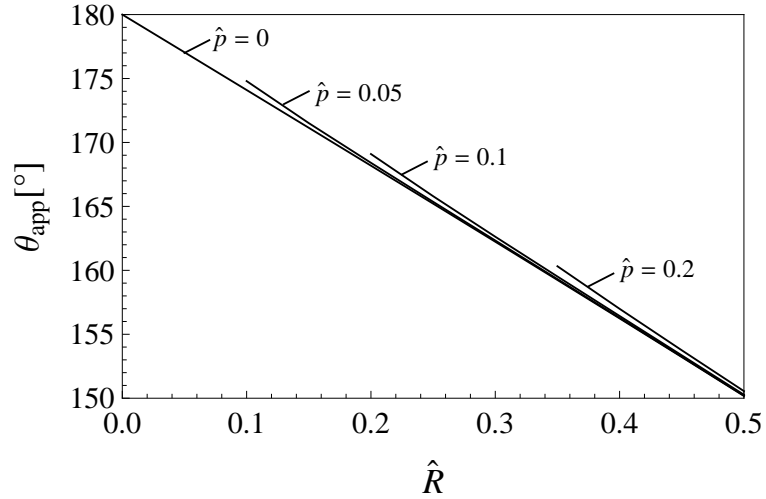

FIG. 13: The apparent contact angle θ_{app} as a function of the radius $\hat{R}$. Results are shown for cylindrical pillars and different dimensionless drop pressure $\hat{p}$.

less pronounced.

V.   DISCUSSION AND DESIGN SUGGESTIONS

Very robust super-hydrorepellent surfaces should possess the ability to support large drop pressures, and should also allow the drops to easy abandon the substrate, roll on it with almost zero contact angle hysteresis, or even easily bounce on it. As already stated, these properties are very desirable in applications such as micro-fluidic-chips and micro-chemical reactors, where drops have to be easily moved and positioned. But, also at the macro-

17

scale, they represent a strict requirement for self-cleaning windows, water-hydrorepellent windshields, or even hydrorepellent clothing. In these latter cases, the droplet pressure may reach large values as a consequence of large inertia forces due to the impact of rain drops. As an example, assuming the rain drop falls at the speed of about $v_0 = 10$ m/s we can easily estimate the maximum impact pressure $p_{max} \approx \rho v_0^2 = 1 \times 10^5$ Pa. Therefore, a self-cleaning super-hydrorepellent window should be necessarily characterized by large values of the critical Wenzel pressure such that $p_W > p_{max}$. Thus, assuming that the substrate is constituted of hemispherical topped cylindrical pillars distribution, and recalling Eq. (19) we found

$$\lambda < \hat{p}_W \frac{\gamma_{LA}}{p_{max}} = -\cos\theta_e \frac{\pi \hat{R}/2}{1 - \pi \hat{R}^2/4} \frac{\gamma_{LA}}{p_{max}} = \lambda_{max} \qquad (20)$$

So taking for $\hat{R}$ the value 0.5, recalling that the liquid-water surface tensions is $\gamma_{LA} \approx 72 \times 10^{-3}$ J/m^2, and assuming a thermodynamic contact angle $\theta_e = 109°$, one ends up with the value $\lambda < 230$ nm, i.e. nanotube forests [20] should be employed in such applications, provided that the pillar height is sufficiently large to avoid direct contact between the free liquid-air interface and the bottom of the solid surface (we also observe incidentally that nanometer spacing between the pillar is also necessary not to alter the transparency of the glass). However, we underline that the present paper is focused on steady-state conditions and a correct treatment for impactig drops should take in account that the curvature of the free surface is determined by the non uniform pressure distribution at the interface.

In case of conical pillars the critical pressure p_L is determined by the condition that the air-liquid interface touches the pillar forest ground. It has been observed that the pressure $\hat{p}_L$ is always smaller than the critical Wenzel pressure $\hat{p}_W$ calculated for hemispherical and flat topped cylindrical pillars, and approaches this value only for infinitely large values of $\hat{h}$. Therefore, one may be tempted to conclude that if large drop pressures have to be supported, the conical pillar shape is not a viable solution. However, we can easily correct for this by simply slightly modifying the pillar design to turn it in a cylinder with a conical tip on the top, i.e. in a conical topped cylindrical pillar. The new conical pillar design guarantees the same critical Wenzel pressure $\hat{p}_W$ as given by Eqs. (17) or (19), but has the fundamental benefit to present a vanishing or negligibly pull-off pressure $\hat{p}_{out}$. As a consequence, drop on a forest of conical topped cylindrical pillars should not suffer from CA hysteresis, as indeed experimentally observed in Ref. [21], and should be able to easily roll or slide on the substrate or even to bounce on it with very high restitution coefficients. This, should also explain why some biological systems as water striders, which usually walk on the free surface of the water, possess a conically shaped distribution of asperities on their super-hydrorepellent legs [11]. Also note that it is useless to have pillars taller than the minimum height necessary to prevent the contact of the liquid surface with the bottom of the pillars forest, in contrast to what is often asserted, i.e. that the taller the pillars the more the super-hydrorepellence of the surface. The argument, which is usually provided, is that as the pillar height is increased, more energy has to be spent to push the drop in full contact with the substrate. Thus, making pillars taller and taller should lead to a very large resistance against the impalement transition [38]. However, one should observe that this energy can always be provided by the pressure p_W acting inside the drop independently of the pillar height, and that the real critical condition for the transition to the Wenzel state to occur is $p = p_W$. Only in case of very small drops (diameter comparable with the spacing λ between the pillars) the physical scenario may slightly change. In this case, it may be shown that the pillar height can actually play an additional role: because of mass conservation, an

additional resistance against impalement transition and drop penetration is generated [22].

VI. CONCLUSIONS

In this paper the behaviour of a liquid drop on super-hydrorepellent surfaces constituted of periodic distribution of pillars has been analyzed. In particular the critical drop pressure p_W which destabilize the fakir-droplet state causing a transition to a Wenzel (full contact) state and the critical pressure p_{out} which causes the detachment of the drop from the substrate have been studied for three types of periodic micro-structured surfaces: conical, hemispherical topped and flat topped cylindrical pillars, regularly disposed on a rigid substrate. Both p_W and p_{out} are equally important to assess the superhydrorepellent properties of surfaces. In fact high p_W values are requested in all those applications in which very high pressures must be supported, e.g. self-cleaning glasses and super-hydrorepellent windshields, whereas small values of p_{out} are desirable to guarantee very small contact angle hysteresis and allow the drop to easily move on the substrate (e.g. microfluidic chemical reactor, micro-fluidic-chips) or, in case of impacting drops, easily rebound from it (e.g. self-cleaning windows, super-water-repellent windshields and biker helmet visors). We have shown that the conical pillars have a pull-off pressure p_{out} vanishing small (that is an advantage in those applications in which liquid drops have to be easily removed from the surface), but the Cassi-Baxter state is destabilized for pressures smaller than the critical value p_W found for hemispherical or flat topped cylindrical pillars. However, a surface microstructured with cylindrical pillars with conical tips would have both advantages of large pressure p_W and zero pull-off pressure p_{out}. Finally, the effect of the pressure on the apparent contact angle θ_{app} has been studied. The analysis has shown that θ_{app} reduces significantly with the pressure in case of conical pillars (in agreement with previous experimental observation), whereas it slightly increases for hemispherical or flat topped cylindrical pillars.

---

[1] Alberti G., DeSimone A., Wetting of rough surfaces: a homogenization approach, Proceedings of The Royal Society of London Series A-Mathematical Physical and Engineering Sciences, **461** (2053), 79-97 (2005).

[2] Barthlott W., Neinhuis C., Purity of the sacred lotus or escape from contamination in biological surfaces, Planta **202**, 1-8 (1997).

[3] Bittoun E. and Marmur A., Optimizing Super-Hydrophobic Surfaces: Criteria for Comparison of Surface Topographies, Journal of Adhesion Science and Technology, **23**, 401-411 (2009).

[4] Blossey R., Self-cleaning surfaces - virtual realities, Nature Mater. **2**, 301 (2003)

[5] Callies M., Chen Y., Marty F., Pepin A., Quere D., Microfabricated textured surfaces for super-hydrophobicity investigations, Microelectronics Engineering, **78-79**, 100-105 (2005).

[6] Callies M., Quere D., On water repellency, Soft Matter, **1** (1), 55-61 (2005)

[7] Cassie A.B.D., and Baxter S., Wettability of porous surfaces, Trans. Faraday Soc. **40**, 546-551 (1944)

[8] Carbone G., Mangialardi L., Hydrophobic properties of a wavy rough substrate, the European Physical Journal E-Soft Matter **16** (1), 67-76 (2005).

[9] Duparrè A., Flemming M., Steinert J., and Reihs K., Optical coatings with enhanced roughness for ultra-hydrophobic, low scatter applications, OIC 2001, Banff, Canada, July 15-20 (2001).

[10] Feng L., Li S.H., Li Y.S., Li H.J., Zhang L.J., Zhai J., Song Y.L., Liu B.Q., Jiang L., Zhu D.B., Super-Hydrophobic Surfaces: From Natural to Artificial, Adv. Mater., **14** (24), 1857 (2002)

[11] Gao X. F., and Jiang L., Water-repellent legs of water striders, Nature, **432** (4), 36 (2004).

[12] Gao X. F., Yan X., Yao X., Xu L., Zhang K., et al, The dry-style antifogging properties of mosquito compound eyes and artificial analogues prepared by soft lithography. Adv. Mater. **19**, 2213–15 (2007)

[13] Gau H., Herminghaus S., Lenz P., Lipowsky R., Liquid Morphologies on Structured Surfaces: From Microchannels to Microchips, Science **283**, 46 (1999)

[14] Herminghaus S., Roughness-induced non-wetting, Europhys. Lett., **52** (2), 165-170 (2000)

[15] Joanny J.F., de Gennes P.G., A model for contact angle hysteresis, Journal of Chemical Physics, **81** (1), 552-562 (1984)

[16] Lafuma A., and Quéré D., Superhydrophobic states, Nature Mater. **2**, 457 (2003)

[17] Swain P.S. and Lipowsky R., Contact Angles on Heterogeneous Surfaces: A New Look at Cassie's and Wenzel's Laws, Langmuir **14**, 6772-6780 (1998).

[18] Liu B. and LAnge F.F., Pressure induced transition between superhydrophobic states: Configuration diagrams and effect of surface feature size, Journal of Colloid and Interface Science, **298**, 899-909 (2006).

[19] Lobaton E.J. and Salamon T.R., Computation of constant mean curvature surfaces: Application to the gas–liquid interface of a pressurized fluid on a superhydrophobic surface, Journal of Colloid and Interface Science, **314**, 184-198 (2007).

[20] Lau K. K. S., Bico J., Teo K. B. K., Chhowalla M., Amaratunga G. A. J., Milne W. I., McKinley G. H., and Gleason K. K., Superhydrophobic Carbon Nanotube Forests, Nano Letters, **3** (12), 1701-1705 (2003).

[21] Martines E., Seunarine K., Morgan H., Gadegaard N., Wilkinson C. D. W., and Riehle M. O., Superhydrophobicity and Superhydrophilicity of Regular Nanopatterns, Nano Letters, **5** (10), 2097-2103, (2005)

[22] Moulinet S., and Bartolo D., Life and death of a fakir droplet: Impalement transitions on superhyrophobic surfaces, Eur. Phys. J. E, **24**, 251-260 (2007).

[23] Neumann A.W. and Good R.J., Thermodynamics of contact angle, Journal of Colloid and Interface Science, **38** (2), 341-358 (1972).

[24] Su Y., Ji B., Huang Y., Hwang K., J. Mater. Sci. **42**, 8885 (2007).

[25] Nosonovsky M. and Bhushan B., Energy transitions in superhydrophobicity: low adhesion, easy flow and bouncing, J. Phys.: Condens. Matter **20**, 395005 (6pp) (2008).

[26] Bartolo D., Bouamrirene F., Verneuil E., Buguin A., Silberzan P., Moulinet S., Europhys. Lett., **74** (2), pp. 299–305 (2006)

[27] Nosonovsky M. and Bhushan B., Biomimetic Superhydrophobic Surfaces: Multiscale Approach, Nano Letters **7** (9), 2633-2637 (2007).

[28] Nosonovsky M., Multiscale Roughness and Stability of Superhydrophobic Biomimetic Interfaces, Langmuir **23**, 3157-3161 (2007).

[29] Nosonovsky M. and Bhushan B., Roughness-induced superhydrophobicity: a way to design non-adhesive surfaces, J. Phys.: Condens. Matter **20**, 225009 (30pp) (2008).

[30] Bhushan B., Nosonovsky M. and Jung Y. C. Towards optimization of patterned superhydrophobic surfaces, J. R. Soc. Interface **4**, 643-648 (2007).

[31] Nosonovsky M. and Bhushan B., Wetting of rough three-dimensional superhydrophobic surfaces, Microsyst Technol **12**, 273–281 (2006).

[32] Patankar N., On the Modeling of Hydrophobic Contact Angles on Rough Surfaces, Langmuir **19**, 1249-1253 (2003).

[33] Patankar N., Hydrophobicity of Surfaces with Cavities: Making Hydrophobic Substrates from Hydrophilic Materials?, Journal of Adhesion Science and Technology **23**, 413–433 (2009).

[34] Nakajima A., Fujishima A., Hashimoto K., and Watanabe T., Preparation of Transparent Superhydrophobic Boehmite and Silica Films by Sublimation of Aluminum Acetylacetonate, Adv. Mater. **11** (16), 1365 (1999).

[35] Nakajima A., Hashimoto K., and Watanabe T., Transparent Superhydrophobic Thin Films with Self-Cleaning Properties, Langmuir, **16**, 7044 (2000).

[36] Onda T., Shibuichi S., Satoh N., and Tsujii K., Super-Water-Repellent Fractal Surfaces, Langmuir, **12** (9), 2125-2127 (1996).

[37] Quéré D., Rough ideas on wetting, Physica A **313,** 32 (2002)

[38] Quéré D., Wetting and Roughness, The Annual Review of Materials Research, **38**, 71-99 (2008)

[39] Quéré D., Lafuma A., and Bico J., Slippy and sticky microtextured solids, Nanotechnology **14**, 1109–1112 (2003)

[40] Richard D., and Quéré D., Bouncing water drops, Europhys. Lett., **50** (6), 769–775 (2000).

[41] Shibuichi S., Onda T., Satoh N., and Tsujii K.,Super Water-Repellent Surfaces Resulting from Fractal Structure, J. Phys. Chem., **100**, 19512-19517 (1996).

[42] Washizu M., Electrostatic Actuation of Liquid Droplets for Microreactor Applications, IEEE Trans. Ind. Appl., **34** (4), 732, (1998).

[43] Wenzel R. N., Surface Roughness and Contact Angle, Ind. Eng. Chem. **28**, 988-994 (1936)

[44] Yang C., Tartaglino U. and Persson B.J.N., Nanodroplets on rough hydrophilic and hydrophobic surfaces, Eur. Phys. J. E, **25,** 139-152 (2008).

[45] Zheng Q.S., Yu Y. and Zhao Z.H., Effects of Hydraulic Pressure on the Stability and Transition of Wetting Modes of Superhydrophobic Surfaces, Langmuir **21**, 12207-12212 (2005).